Atmos. Chem. Phys. Discuss., 15, 24909–24953, 2015
www.atmos-chem-phys-discuss.net/15/24909/2015/
doi:10.5194/acpd-15-24909-2015

Atmospheric Chemistry and Physics Discussions

The millennium water vapour drop in chemistry-climate model simulations

S. Brinkop[1], M. Dameris[1], P. Jöckel[1], H. Garny[1], S. Lossow[2], and G. Stiller[2]

[1]Deutsches Zentrum für Luft- und Raumfahrt (DLR), Institut für Physik der Atmosphäre, Oberpfaffenhofen, Germany
[2]Karlsruher Institut für Technologie (KIT), Institut für Meteorologie und Klimaforschung, Karlsruhe, Germany

Received: 11 August 2015 – Accepted: 25 August 2015 – Published: 14 September 2015

Correspondence to: S. Brinkop (sabine.brinkop@dlr.de)

Published by Copernicus Publications on behalf of the European Geosciences Union.

Abstract

This study investigates the abrupt and severe water vapour decline in the stratosphere beginning in year 2000 (the "millennium water vapour drop") and other similar stratospheric water vapour drops by means of various simulations with the state-of-the-art Chemistry-Climate Model (CCM) EMAC (ECHAM/MESSy Atmospheric Chemistry Model). The CCM EMAC is able to reproduce the signature and pattern of the water vapour disturbances in agreement with those derived from satellite observations. Model data confirm that this extraordinary water vapour decline is in particular obvious in the tropical lower stratosphere. The starting point of the severe water vapour drop is identified in the tropical lower stratosphere and the start date is found to be in the early days of 2000. We show that the driving forces for this significant drop in water vapour mixing ratios are tropical sea surface temperature changes due to a preceding strong El Niño–Southern Oscillation event (1997/98), which was followed by a La Niña and supported by the prevailing western phase of the equatorial stratospheric quasi-biennial oscillation (QBO) at that time. This constellation of ENSO and QBO obviously lead to the outstanding anomalies in meteorological quantities which are identified in the equatorial atmosphere: (a) a distinct warming (up to 1 K) of the tropical upper troposphere (200 to 120 hPa) beginning in mid-1997 and lasting for about one and a half years, (b) a strong warming (up to 2.5 K) of the tropical lower stratosphere (100 to 50 hPa), beginning in early 1999 and ending in early 2000, and (c) a significantly enhanced upwelling at the tropopause in the late 1990s and an obviously reduced upwelling around the year 2000 followed by a period of enhanced upwelling again. These dynamically induced changes are unambiguously connected to the stratospheric water vapour anomaly. Similarly strong water vapour reductions are also found in other years, and seem to be a typical feature after strong combined El Niño/La Niña events, if the QBO west phase has prolonged down to the tropopause.

ACPD
15, 24909–24953, 2015

1 Introduction

Since the early 1980s, balloon-borne stratospheric water vapour measurements (e.g., Hurst et al., 2011) and corresponding satellite measurements starting in the early 1990s (UARS/MLS, UARS HALOE, and SAGE II instruments; see for instance Solomon et al., 2010; Hartmann et al., 2013) an increase of stratospheric water vapour was long reported and climate model simulations uniformly predict a continuous increase of stratospheric water vapour concentrations in the future (SPARC CCMVal, 2010; Stenke and Grewe, 2005). However, if we look from the late 1980s/early 1990s to now, we actually find a decreasing trend from merged satellite observations in the lower stratosphere (see Hegglin et al., 2014). This has become the big conundrum now and there is a lot of discussion if Boulder balloon observations are representative or if there is an issue in the satellite data merging.

An increase in stratospheric water vapour with time is expected as a net result of global warming, including enhanced atmospheric concentrations of methane, which affect water vapour concentrations through methane oxidation. However, the multi-year data sets also show significant fluctuations on different time scales which make it difficult to assess robust trends.

In the year 2000, an extraordinary sudden drop of stratospheric water vapour content has been observed (e.g., Randel et al., 2006; Fueglistaler et al., 2005), which brought again into focus that temperature fluctuations have a large potential to significantly impact the amount of water vapour in the stratosphere. Randel and colleagues showed that the tropical tropopause temperatures were noticeably lower than normal after the drop due to an increase in tropical upwelling.

Since water vapour is the most prominent greenhouse gas, and therefore is an important contributor to variations and trends in climate, it is necessary to better understand its large variability. Stratospheric water vapour variations are connected with temperature changes in the tropical region, especially with the cold-point temperature (Randel et al., 2004; Fueglistaler, 2013). Changes of stratospheric water vapour levels

ACPD
15, 24909–24953, 2015

ranging from inter-annual to decadal time scales are less well understood, in particular the contribution of processes involved. Well-known and understood is the "tape-recorder" effect (Mote et al., 1996) describing the annual cycle of the tropical stratospheric water vapour amount in accordance with the seasonally varying cold point temperature (e.g., Fueglistaler et al., 2005). Moreover, variations of the tropopause temperatures are clearly related to tropical upwelling, the equatorial quasi-biennial oscillation of stratospheric zonal winds (QBO), and the El Niño–Southern Oscillation (ENSO) as for example discussed by Randel et al. (2004). Recent analyses of the observed stratospheric water vapour record show that many of the variations on time scales of one to several years can be linked to changes in tropical tropopause temperatures, but some discrepancies still exist (e.g., Schoeberl et al., 2012; Fueglistaler et al., 2013). Randel and Jensen (2013) state that the water vapour fluctuations observed by satellite instruments over the last 20 years are not adequately reproduced by "free-running" Chemistry-Climate Models (CCMs), although those were forced by observed sea-surface temperatures (SSTs) and concentrations of greenhouse gases and ozone depleting substances were prescribed. Randel and Jensen point out, that current CCMs are not able to reconstruct the severe water vapour drop after the beginning of year 2000. Therefore, they conclude that important components of internal variability might be missing or at least under-represented in the model systems, especially in the tropical tropopause layer (TTL). Similar investigations summarise that it is still unclear whether the inability to simulate the observed trends is due to the large uncertainties in the observed stratospheric water vapour and tropical tropopause temperatures (e.g., Wang et al., 2012), inaccuracies in the CCMs, or whether the models miss relevant mechanisms (see Chapter 4 in WMO, 2014).

Here we present results of a set of simulations with the state-of-the-art chemistry-climate model (CCM) EMAC (**E**CHAM/**M**ESSy **A**tmospheric **C**hemistry model), indicating that it is possible to retrace the observed water vapour fluctuations in the stratosphere (including the millennium drop), if appropriate boundary conditions are applied. The advantage of a CCM is that it includes chemical feedbacks of radiative important

ACPD
15, 24909–24953, 2015

greenhouse gases like ozone, which are important for the stratospheric temperature distribution. In the following section the CCM EMAC is briefly described and the investigated simulations are presented. In Sect. 3 model data are compared to observations. In Sect. 4 three long-term model simulations are analysed, differing mainly with respect to surface temperatures or applied nudging. An overall discussion of our findings is given in Sect. 5.

2 Method and data

2.1 Description of the model system

The ECHAM/MESSy Atmospheric Chemistry (EMAC) model is a numerical chemistry and climate simulation system that includes sub-models describing tropospheric and middle atmosphere processes and their interaction with oceans, land and human influences (Jöckel et al., 2010). It uses the second version of the Modular Earth Submodel System (MESSy2) to link multi-institutional computer codes. The core atmospheric model is the 5th generation European Centre Hamburg general circulation model (ECHAM5, Roeckner et al., 2006). For the present study we analysed EMAC (ECHAM5 version 5.3.02, MESSy version 2.50) in the T42L90MA-resolution, i.e. with a spherical truncation of T42 (corresponding to a quadratic Gaussian grid of approx. 2.8 by 2.8° in latitude and longitude) with 90 vertical hybrid pressure levels up to 0.01 hPa.

The multi-year simulation has been performed with the CCM EMAC in the framework of the ESCiMo project (Earth System Chemistry integrated Modelling, Jöckel et al., 2015). Within ESCiMo so-called reference (RC) simulations have been carried out, as defined by the IGAC/SPARC Chemistry-Climate Model Initiative (CCMI) and described in detail by Eyring and Lamarque (2012). The forcings of the two transient hindcast reference simulations in either free-running (RC1; from 1960 to 2011) or in a nudged mode (RC1SD; from 1980 to 2012) are similar. They are taken from observations or empirical data, including anthropogenic and natural forcings based on changes in trace

ACPD
15, 24909–24953, 2015

gases, solar variability and volcanic eruptions. The quasi-biennial oscillation (QBO) is in all simulations slightly nudged to get the correct phasing of the observed QBO (Jöckel et al., 2015). The sea surface temperatures (SSTs) and the sea ice concentrations (SICs) are from observations or reanalysis data (RC1: HadISST, RC1SD: ERA-interim). In the case of RC1SD the model prognostic variables (vorticity, divergence, the logarithm of the surface pressure, the temperature and additionally the zonal mean temperature (wave number zero in spectral space)) are nudged by Newtonian relaxation towards ERA-Interim reanalysis data. Therefore, the RC1SD simulation can be used to compare the model data with corresponding observations including year-to-year variations. The transient forecast reference simulation (from 1960 to 2100; RC2) is a future projection that follows the IPCC scenario RCP 6.0 and a specified scenario of the development of ozone depleting substances (halogen scenario A1; WMO, 2007). It also considers solar variability in the past and future (for details see Jöckel et al., 2015). Because of potential discontinuities between the observed and simulated data record, RC2 uses SSTs and SICs derived from a coupled climate model simulation (with an interactive ocean, HadGEM2, RCP6.0 scenario; Johns et al., 2011) for the entire period. In the following analysis we confine the data of the RC2 simulation from 1960 to 2040.

2.2 Observational data sets

To analyse different characteristics of the millennium drop in water vapour we use besides the EMAC simulation with specified dynamics RC1SD also a combination of satellite observations performed by HALOE (Halogen Occultation Experiment) and MIPAS (Michelson Interferometer for Passive Atmospheric Sounding) instruments (Russell et al., 1993; Fischer et al., 2008).

Previous analyses of the millennium drop characteristics focused mainly on its absolute value (Randel et al., 2006; Maycock et al., 2014), i.e. those studies used the water vapour difference between multi-year means before 2000 and after 2001. Those approaches reflected mainly the change in the large-scale circulation that contributed

ACPD
15, 24909–24953, 2015

to the millennium drop. Contributions from the QBO and ENSO on the other hand were attenuated or even completely removed. Here, we rely on running annual means to make the contributions of these two variability patterns more visible. We focus on several characteristics of the millennium drop as a function of altitude and latitude. Based on derived start and end dates we calculate the length of the drop, and the total change in water vapour. For more details see the Appendix.

3 The millennium water vapour drop

This study is motivated by a chart which is shown in Fig. 1 (the original figure was published by Randel and Jensen, 2013): The near-global lower stratospheric water vapour anomalies were derived from multi-year satellite measurements (1992–2012) at the 83 hPa pressure level (approximately 17 km altitude). It impressively indicates inter-annual fluctuations of up to 15 % (about 0.5 ppmv) from the 20 year mean mixing ratio. There are clear signs of the QBO over the full time period. The figure highlights the severe water vapour drop (approximately −0.7 ppmv) in the year 2000. In Fig. 1 we show that our RC1SD simulation (with specified dynamics) is able to closely reproduce the water vapour fluctuations as observed, here representing the near-global mean (60° S–60° N) anomalies. Except for the time before 1994, where the eruption of Mt. Pinatubo had a significant impact on temperature and water vapour, the temporal evolution of water vapour at the pressure level 83 hPa by RC1SD is in accordance with observed values. For example the timing of relative minimum and maximum water vapour values is reproduced very well. Evidently the model underestimates the strength of the inter-annual fluctuations (only about 0.3 ppmv instead of 0.5 ppmv). The severe drop in 2000 is slightly underestimated (about −0.12 ppmv), yet the period with lower than normal water vapour is captured well. The deviations after 2006 can partly be attributed to the corresponding positive anomalies of the cold point temperature in the tropical region (Fig. 2). The cold point temperature anomalies are represented better than the

ACPD
15, 24909–24953, 2015

moisture anomalies, likely due to the direct nudging of zonal mean temperature in the model to ERA-Interim.

We conducted an additional simulation similar to RC1SD, but without nudging of zonal mean temperature (RC1SDNT). The RC1SDNT simulation shows a cold point temperature anomaly time series similar to RC1SD, but the water vapour anomalies are by a factor of about 1/3 too small (not shown). The lower absolute values of the anomalies are likely caused by a mean tropical cold point tropopause temperature (189.4 K) which is lower than for RC1SD (192.1 K) within the 1992–2012 period. We know from model inter-comparison studies that it is a common feature of many models, that the cold point tropopause in the tropics has a cold bias (Gettelman et al., 2009). We conclude that in order to correctly simulate water vapour anomalies in time and amplitude, it is important not only to correctly reproduce the temperature anomaly, but also the mean temperature at the cold point tropopause.

There are expectations that the water vapour drop in observations exhibits different characteristics at different latitudes and altitudes with respect to the start date, the strength and the length of the anomaly. For example, Urban et al. (2014) show that in the tropics the significant reduction of water vapour started in the altitude range from 16.5 to 18.5 km (375–425 K) in early 2000, whereas between 25 and 30 km (625–825 K) it began in late 2001. Moreover, they demonstrate that the drop was more pronounced in the lower tropical stratosphere than in the middle stratosphere, i.e. −1.3 and −0.6 ppmv, respectively. The minimum water vapour mixing ratios were found in the lower stratosphere about one year, in the middle stratosphere almost two years after the onset of the drop.

A more comprehensive and novel analysis is provided in Fig. 3. The characteristics of the water vapour drop with respect to strength, drop length and drop date are shown as a function of latitude and altitude. The amplitude of the drop maximises in the tropical lower stratosphere consistently in observations and the RC1SD simulation. However the amplitude in the tropics is 50 % larger in the observations. Towards higher latitudes and altitudes up to about 20 hPa the drop amplitude typically decreases. Above

ACPD
15, 24909–24953, 2015

this level some increase in the drop amplitude can be observed that goes along with a stronger QBO variability. It is unclear if the drop amplitude here can be unambiguously attributed to the millennium drop or simply reflects natural QBO variability or a combination of both.

A similar pattern can be seen for the start date of the millennium drop. Up to 40 hPa the drop occurs in most cases during the year 2000. Above 30 hPa there is a clear shift to dates in 2002 and 2003, again mostly controlled by QBO variability. The stronger branch of the Brewer–Dobson circulation on the Northern Hemisphere is clearly visible in the earlier start dates of the drop compared to the Southern Hemisphere.

The drop length is the less consistent parameter. Values typically range from 6 months (inherent from the approach) to about 20 months. In the simulation the length is in the order of 9 months in the lowermost tropical stratosphere. The observations exhibit here longer drops related to the larger drop amplitudes.

4 The millennium water vapour drop in other ESCiMo simulations

In the last Section, we showed that the millennium water vapour drop is reasonably well reproduced by an EMAC simulation in the nudged mode. In the following we investigate whether also free-running simulations are capable to simulate the variability in lower stratospheric water vapour, and in particular the drop in year 2000.

The magnitude of inter-annual variability in water vapour in the tropical lower stratosphere is overall far lower in the free-running RC1 and RC2 simulations (Fig. 4). However, a decrease in water vapour around the year 2000 is found also in RC1. The strength of the drop is underestimated by a factor of 2. RC2 does not show a drop at all. Furthermore, RC1 and RC2 both have a time lag compared to RC1SD and are not able to simulate the long period with low water vapour values after 2000. Interestingly a different picture shows up for the simulated cold point temperature anomalies (Fig. 5), which are comparable for RC1SD and RC1 and only slightly smaller for RC2. Similar to the water vapour drop, the cold point temperature drop lags behind the year 2000

ACPD
15, 24909–24953, 2015

(Fig. 5), which points to a shift in the incidence of temperature relevant processes: El Niño and corresponding large-scale upwelling, the radiative effect due to the local ozone distribution and the QBO (Randel and Jensen, 2013).

5 Other "drops" of moisture anomalies in the lower stratosphere and their relation to preceding El Niño/La Niña events

The millennium drop in water vapour 2000/01 after the strong 1997/98 El Niño event is followed by an unusual long time period of relatively low water vapour values (Fig. 1). Since Solomon et al. (2010) found that these anomalous low water vapour values in the lower stratosphere caused a reduced trend in global surface temperatures over the years 2000–2009 by about 25 %, we wonder, if this millennium drop is unique or if we can expect that such a drop is a more or less typical feature of stratospheric water vapour variability? Is there a relation to preceding El Niño/La Niña events? The El Niño Southern Oscillation is an ocean–atmosphere feedback that occurs every 2–5 years and propagates throughout the troposphere into the lower stratosphere. Therefore El Niño/La Niña events have the potential to couple the surface temperature with the stratosphere.

We have analysed the time evolution of water vapour anomalies for the RC1SD and RC1 simulations at 80 hPa (Fig. 6) for the full time period available for the respective simulations. In the RC1 simulation we found 5 and in the RC1SD simulation 3 relatively large water vapour drops marked by a red asterisk, which are comparable to the millennium drop amplitude in the respective simulation. An additional asterisk marks a smaller water vapour drop after the 1986/87 El Niño in RC1SD, which additionally was examined.

Because the amplitudes in the RC1 simulation are generally smaller than in RC1SD, we define a "large drop" in the simulations differently: RC1SD: drop > 0.5 ppmv, and for RC1: drop > 0.2 ppmv.

ACPD
15, 24909–24953, 2015

Although there are 2 other large water vapour drops in the RC1SD simulation starting 1994 and 1996, we neglect this time period, because the eruption of Mt. Pinatubo (1991) had a significant impact on temperature and water vapour. Through the use of nudging data from reanalysis the effect of Mt. Pinatubo is partially captured in the dynamics and the temperature field. In another sensitivity study with the RC1 simulation set-up, which includes the effect of the Mt. Pinatubo eruption in terms of additional aerosols in the stratosphere, a strong positive water vapour anomaly lasting over 5 years is found, followed by a huge water vapour drop (Fig. 6, red curve). Likewise, we cannot exclude, that the eruption of Mt. Chichon in 1982, although less strong than the eruption of Mt. Pinatubo had an influence on the results.

The dominant effect of El Niño/La Niña events on the tropical surface temperatures (including land and sea surface temperatures) are clearly visible in Fig. 7 in all simulations. The data derived from the RC1 simulation indicate strong temperature signals related to the El Niño and La Niña episodes (1: 1969/70, 2: 1973/74, 3: 1982/83, 4: 1986/87, 5: 1997/98, 6: 2009/10). The RC1SD simulation only covers El Niño and La Niña events from no 3 to no 6, but the surface temperatures are similar to RC1. The 1997/98 El Niño event (5) was unusually strong compared to former events, with a tropical surface temperature amplitude of about 0.7 K, similar for both RC1 and RC1SD. Case no 4 shows a two year lasting El Niño starting as weak in 1986 and becoming 1987/88 a moderate event followed by a strong La Niña. The SSTs for the RC2 simulation were taken from a coupled ocean–atmosphere simulation of the HadGEM-model, and the tropical surface temperatures are generally lower than in observations (Fig. 7b). However, the simulated surface temperature represent similar fluctuations (in magnitude) as observed, but originating in different periods of time and often with longer time duration. A causal relationship between large drops and preceding El Niño/La Niña events could not be found.

In order to understand the origin of large water vapour declines, we analysed the corresponding development and incidence of two important components of natural variability influencing the temperature in the TTL: the El Niño/La Niña events and the QBO.

ACPD
15, 24909–24953, 2015

The QBO appears as a reversal of the tropical zonal wind direction with a mean period of about 28 months (ranging from 22 to 34 months) and is a primarily wave-driven stratospheric phenomenon. In the tropical lower stratosphere the QBO is the dominant dynamic feature.

As mentioned above (Sect. 2), in all three EMAC simulations the QBO is nudged to zonal mean winds with respect to the amplitude and phase. Therefore the signature of the QBO in the temperature anomaly (Fig. 8b, RC1 as representative for all simulations) propagating downwards to the TTL is present in all three EMAC simulations.

It is well-known (Rosenlof and Reid, 2008) that the QBO phase contributes to the extraordinary temperature fluctuation in the tropical tropopause region around year 2000 due to an unusual long QBO-phase: strong east-winds in the equatorial lower stratosphere (around 30 hPa) were persistently detected for nearly two years (2000/01); the downward propagation of the zero-wind line (change from east- to west-wind direction) stopped for one year (from mid-2000 to mid-2001) at about 40 hPa.

Around a strong El Niño event (black vertical lines, Fig. 8) we find a positive moisture and temperature anomaly throughout the troposphere up to about 100 hPa. Above, in a narrow layer between 100 and 50 hPa (marked with dashed black lines) a negative temperature anomaly occurs, except for the 1982/83 El Niño, where a positive QBO phase with warming probably masks this feature. For the 1997/98 and the 2009/10 El Niño the cooling is not pronounced, but also visible. Positive and negative temperature anomalies in the narrow layer are related to a large part by changes in upwelling, which directly modifies tropopause temperatures through lifting of air masses and corresponding advection of ozone anomalies into the TTL. A positive upwelling anomaly (cooling) is accompanied by a negative ozone anomaly (cooling). Therefore, upwelling anomaly and ozone anomaly are highly anti-correlated with a Pearson's correlation coefficient $R = -0.6$ at 70 hPa for both RC1 and RC1SD (Table 1). Tropical upwelling is calculated from the model data in terms of the residual vertical velocity w^* as introduced in the transformed Eulerian mean (TEM) equations (e.g. Holton, 2004). As expected temperature and large-scale upwelling are also strongly anti-correlated with a Pear-

ACPD
15, 24909–24953, 2015

son's correlation coefficient $R = -0.7$ (70 hPa) for RC1SD (RC1: $R = -0.58$) (Table 1). Likewise temperature and QBO are positively correlated with $R = 0.5$ (RC1) ($R = 0.4$ for RC1SD) at 70 hPa. The correlation coefficients decrease towards 90 hPa because the effect of the QBO on temperature decreases.

In the TTL positive temperature anomalies result in positive water vapour anomalies propagating upward into the stratosphere (Fig. 8a). They are an indicator of the regional dynamical properties (Mote et al., 1996; Randel et al., 2004). The traveling time for water vapour in the lower stratosphere calculated from the maximum correlation between temperature at 100 hPa and water vapour at 82 hPa is 2 months according to Rosenlof and Reid (2008).

We find a similar result only for RC1SD, but RC1 and RC2 exhibit the maximum correlation for lag = 0. Consistently, upwelling is smallest in the RC1SD and largest in the RC1 simulation leading to a faster transport of water vapour through the TTL in RC1. Accordingly, the correlation between temperature and moisture at 70 hPa is stronger for RC1 ($R = 0.8$) than for RC1SD ($R = 0.4$).

We use this connection to analyse the conditions under which large temperature drops occur, in order to understand the origin of large water vapour drops. In doing so, we disregard other processes that may contribute to the water vapour distribution and its variability in the TTL such as convective and large-scale water vapour transports, ice supersaturated regions and cirrus development.

Every El Niño event is generally accompanied by a strong positive upwelling anomaly (Fig. 9) followed by a period with reduced upwelling and thus positive temperature anomalies in the TTL. Many of these positive temperature anomalies mark the onset of strong drops in temperature and water vapour. Note the double maximum in the temperature anomaly after the 1972/73 (no 2) El Niño (Fig. 8b), which is related to the reduced upwelling in Fig. 9. This confirms that upwelling plays the other important role in generating temperature anomalies around 100–60 hPa beside the QBO, directly through adiabatic cooling.

ACPD
15, 24909–24953, 2015

Although the SSTs of the RC1SD and RC1 simulation are similar, the period with a positive upwelling anomaly after the year 2001, leading to the observed low tropopause temperatures and low water vapour values in the lower stratosphere (Randel et al., 2006) is not adequately simulated in the RC1 simulation. Interestingly after 2001, where tropical SSTs only exhibit a small but long lasting positive anomaly in both, RC1and RC1SD, upwelling already shows a positive anomaly, stronger in RC1SD than in RC1. This might be related to an enhanced momentum flux convergence in the subtropical region (Randel et al., 2006), but a detailed analysis of our simulations regarding this topic is beyond the scope of this study.

If a strong El Niño plus La Niña event is typically followed by a large temperature/water vapour drop we might expect that typical conditions exist that favour these large variations. We performed an episode analysis for the previously selected 4 (RC1SD) and 5 (RC1) strong El Niño events, followed by a La Niña event (Fig. 7), respectively. The onset of the individual temperature drops at 80 hPa (Fig. 10) is placed at month 0, so that the periods before the drop and afterwards can be consistently analysed. We selected the start of the temperature drop (rather than the drop in water vapour), where temperature is at its maximum, for the definition of the corresponding event, because QBO, upwelling and ozone have a direct effect on temperature. Water vapour anomalies follow temperature anomalies directly or with a time lag.

The onset of the millennium water vapour drop (Fig. 11, green dashed line) is phase shifted by 3 to 4 months and the 2009/10 water vapour drop about 2 months after the temperature maximum of the respective drops (Fig. 10). For the other drops in RC1SD and all drops in RC1, we find no time lag.

All onsets of the temperature drops of RC1SD and RC1 are associated with a minimum in the large-scale upwelling anomaly (Fig. 12), accompanied by a maximum in ozone anomaly (Fig. 13) and for RC1SD only, a west-phase of the QBO (Fig. 14). Accordingly, the minima of the drops show maxima in upwelling, minima in ozone and an east-phase of the QBO (for RC1SD only).

ACPD
15, 24909–24953, 2015

RC1 does not show the transition from west QBO to east QBO phase at the 80 hPa level as a typical feature, because the QBO-phases do not propagate down as far into the TTL as in RC1SD. Therefore, the contribution of the QBO phase to the drop is less for RC1.

Generally, the correlation between temperature anomaly and QBO anomaly is smaller in RC1 than in RC1SD for the 90 hPa level compared to 70 hPa (Table 1). This points to a different coincidence of upwelling and QBO in RC1, which might partly explain, why the anomalies in temperature and hence water vapour at TTL level are smaller in RC1.

The time evolution of the upwelling anomaly is strongly correlated with SST anomalies during El Niño and La Niña periods (El Niño region 3.4, Figs. 15 and 16) except for the 1982/83 (no 3) El Niño event, which had its maximum already before the maximum of surface temperature was reached. However, for the whole simulation period in RC1SD upwelling anomalies and surface temperature anomalies in the tropics are only correlated with $R = -0.4$. We conclude, that under most El Niño/La Niña conditions the high SST anomalies have the dominant influence on upwelling maxima and minima, and thus on the drop amplitude, whereas under normal SST conditions the influence on upwelling is smaller.

Both simulations, RC1SD and RC1, show variable time-lags between El Niño (in terms of SST anomaly maximum) and temperature drop (represented by the negative anomaly in upwelling) onset ranging from 6 to 34 months, which is a result of the SST time evolution during the El Niño/La Niña phases. The relationship is particularly visible in Fig. 16 for the 1972/73 (no 2) El Niño, which was followed by a 2 year long-lasting La Niña event and had the longest analysed time lag.

6 Summary and discussion

We demonstrated that observed fluctuations and changes of lower stratospheric water vapour content can be reproduced by multi-year CCM simulations, if specific boundary

ACPD
15, 24909–24953, 2015

conditions are met. The nudged simulation (RC1SD) fits best with observations regarding the time evolution of lower stratospheric water vapour and its amplitude. In contrast, the free-running RC1 and RC2 simulations provide too small amplitudes and thus too low variability in water vapour.

The analyses of these three model simulations show that the observed millennium water vapour drop is driven mainly by two forcings, namely an unusual strong positive tropical SST anomaly (from El Niño 1997/98) coinciding with a negative phase of the QBO in the years before the drop. This is followed by negative tropical SST fluctuations (from La Niña 1999/2000) with reduced upwelling and a positive phase of the QBO. After the year 2000, we find a period of stronger than usual upwelling and a corresponding negative temperature anomaly.

Strong drops in temperature and water vapour at the tropopause and above can be found also after other El Niño events (e.g. 1986/87 and 2009/10) followed by a La Niña, when conditions comparable to the millennium drop occur: Reduced upwelling due to a La Niña event in coincidence with a west phase of the QBO (warming) followed by an increase in upwelling in connection with the east phase of the QBO (cooling). The reduced upwelling induces a positive ozone anomaly (warming) and vice versa. Interestingly, from the RC1 simulation, we experience that the contribution of the QBO to a temperature or water vapour drop is small. The smaller temperature and thus water vapour amplitudes in RC1 seem to be a result of the smaller QBO contribution to the drop compared to the RC1SD simulation (Fig. 14). We conclude that it is the coincidence of upwelling and QBO that controls the strength of the temperature and the corresponding moisture drop.

During the periods of strong surface forcing of a successive El Niño/La Niña event, the trend in the upwelling anomaly is strongly correlated to the SSTs in the El Niño 3.4 region (Figs. 15 and 16). The time it takes to shift from El Niño to La Niña determines the time the temperature drop lags the El Niño maximum.

The strong and widely noticed water vapour drop in the year 2000 is particularly remarkable due to the fact, that it is followed by a 5 year period of low stratospheric humid-

ACPD
15, 24909–24953, 2015

ity. This cold period after 2000 is accompanied by stronger than usual tropical upwelling between the tropopause and 70 hPa (Fig. 9), causing the low temperatures and thus the low water vapour in the lower stratosphere, as described in Randel et al. (2006) and Rosenlof and Reid (2008). These negative water vapour anomalies after 2001 lead to a reduction in the global surface temperature warming trend of 25 % (Solomon et al., 2010). Therefore, it is important to correctly model the relevant processes leading to the observed variations in moisture in the lower stratosphere. From our 3 ESCiMo simulations RC1SD (nudged), RC1, and RC2 we found that only the RC1SD simulation reproduces this millennium drop and the period with low water vapour values after year 2000 in accordance with observations. RC1 and RC2 simulate too small amplitudes in water vapour and RC1 a slightly different timing of the drop onset. RC2 shows no strong drop at all. Furthermore RC1 and RC2 both do not capture this period with low water vapour values, and thus the important contribution of the lower stratospheric water vapour feedback in RC1 is underrepresented.

Tropical upwelling, that strongly controls temperature in the tropopause layer, is influenced both by the ENSO (see e.g. Calvo et al., 2010) and the QBO. We find that in the free-running simulations (RC1, RC2) the QBO does not propagate downward far enough to influence the upwelling in the tropopause region. Furthermore, the relation of tropical SSTs/ENSO to upwelling is stronger in RC1 compared to the nudged simulation.

This raises the question, whether there are processes or forcings, which are missing or underrepresented in the RC1 and the RC2 simulations. Because SSTs are prescribed from similar observations, RC1SD and RC1 differ mainly with respect to the nudging (of temperature, vorticity, divergence, the logarithm of surface pressure), and the temperatures of land surfaces, which are not prescribed, but can evolve interactively. RC2 uses simulated SSTs, which are colder than those used for RC1. Therefore RC2 can be expected to show different results at least for the time evolution.

EMAC is a CCM which considers interactively the feedback of dynamics, chemistry and radiation, including parameterisations for sub-grid scale processes. Global mod-

ACPD
15, 24909–24953, 2015

els like EMAC resolve the large-scale circulation, but unresolved convective transport effects or the drag due to breaking gravity waves are considered only through parameterisations. The response of the free-running model system to the prescribed SSTs appears to differ from the nudged model, i.e. the response in the reanalysis. Deckert and Dameris (2008) showed that higher SSTs in the tropics amplify deep convection locally with subsequent more convective excitation of quasi-stationary waves. These waves propagate upward and can dissipate in the UTLS, carrying the signal into the low-latitude lower stratosphere. An increase of SSTs intensifies the activity of tropical convection, which strengthens the associated latent-heat release and warms the tropical upper troposphere. Consequently, the meridional temperature gradient is increased, which strengthens and shifts the subtropical jets to higher latitudes. Waves can propagate further up and break at higher levels leading to stronger upwelling (Shepherd and McLandress, 2011).

These findings with respect to tropical dynamics and the involved mechanisms influencing the transmission from disturbances originating near the surface, propagating through the troposphere and affecting the UTLS region suggest that these processes may not adequately be represented by the EMAC model. So far it is not clear, how many of the processes of the obtained cause and effect relationship are insufficiently described or parameterised. More investigations are needed to clarify, whether an inaccurate representation of these processes and/or feedback mechanisms in EMAC is responsible, or if it is a matter of model resolution that leads to the disagreement regarding the strength of year-to-year fluctuations of water vapour and temperature. Moreover, a general problem of "free running" models is, that the cold point is slightly too high and therefore a little too cold compared to observations, which already leads to a reduced variability in absolute humidity.

Looking at the now 22 year long global water vapour record constructed on satellite-instrument measurements, there is another severe water vapour drop of similar size apparent after 2011 (Urban et al., 2014). Once longer records of global measurements become available in the future, it might turn out that such significant stratospheric water

ACPD
15, 24909–24953, 2015

vapour fluctuations occur regularly. Natural changes that affect the stratospheric water vapour content are modified by climate change itself, may impact future climate. This demonstrates that robust climate predictions need realistic fluctuations of SSTs and an adequate representation of the QBO to reproduce the observed stratospheric water vapour fluctuations. Obviously severe changes can have a "memory" effect, impacting climate change on a decadal time scale (Solomon et al., 2010).

The variability of tropopause temperatures is dominated on an inter-annual period by modulations of the El Niño–Southern Oscillation, the tropical upwelling, and the stratospheric QBO. Variations in ozone amplify the impact of those drivers. In our analysis this relationship seems to be sufficient to show the connection between large water vapour drops, QBO phases, and preceding El Niños. While this part is understood (Randel et al., 2006, 2009; Fueglistaler and Haynes, 2005; Jones et al., 2009; Urban et al., 2012; Fueglistaler et al., 2013; Randel and Jensen, 2013), the connection between temperature and moisture is far more complicated.

From Urban et al., 2014 we know that a period exists, where the variability of lower stratospheric water vapour is not simply explainable by the course in mean zonal temperature (2008–2011). Here, we omitted to analyse this period, because it is beyond the scope of this paper.

We further neglected any possible changes in the transport of water vapour into the TTL, the presence of supersaturated regions or cirrus clouds in the TTL. Since temperature and water vapour are non-linearly dependent, a monthly mean temperature does not give any information about the actual frequency distribution of saturation values of water vapour. In our simulations, the actual water vapour values are generally lower than the saturation values. It points to a lack of certain processes important for the budget of water vapour in the lower stratosphere (for instance convective overshooting). This is a topic of further research.

ACPD
15, 24909–24953, 2015

Appendix A: Millennium drop characteristics

A1 UARS/HALOE

HALOE was deployed on UARS (Upper Atmosphere Research Satellite) and performed measurements from September 1991 to November 2005. The measurements were based on the solar occultation technique. Absorption spectra were obtained in specific spectral bands in the wavelength range between 2.5 and 11 µm. Typically 30 occultations per day were performed, generally at two distinct latitude bands in the opposite hemispheres, based on sunrise and sunset measurements. Within a month the observations covered roughly the latitude range between 60° S and 60° N. Water vapour results were retrieved from the 6.54 to 6.67 µm spectral range, typically covering altitudes from about 10 to 85 km. For the analysis here we use data retrieved with version 19, that have been used extensively (e.g. Kley et al., 2000; Randel et al., 2006; Scherer et al., 2008; Hegglin et al., 2013).

A2 Envisat/MIPAS

To fill some observational gaps that are inherent of the solar occultation technique employed by the HALOE instrument we also consider MIPAS limb observations of thermal emission. Those provided typically more than 1000 individual measurements per day, lasting from June 2002 to April 2012. MIPAS was carried by Envisat (Environmental Satellite) which used a sun-synchronous orbit with full latitudinal coverage on a daily basis. The measurements covered the spectral range between 4.1 and 14.6 µm. Initially a spectral resolution of 0.035 cm^{-1} (unapodised) was used, however after an instrument failure in March 2004 later observations had to be performed with a reduced resolution of 0.0625 cm^{-1} (Fischer et al., 2008). Here we utilise data that have been retrieved with the IMK/IAA (Institut für Meteorologie und Klimaforschung in Karlsruhe, Germany/Instituto de Astrofsica de Andaluca in Granada, Spain) processor. Water vapour information is retrieved from several microwindows in the wavelength range

ACPD
15, 24909–24953, 2015

between 7.09 and 12.57 µm providing data from 10 km up to the lower mesosphere. For the observations with high spectral resolution retrieval version 20, for the low resolution time period version 220 is used. Detailed information on these data sets can be found in Schieferdecker (2015) and Hegglin et al. (2013).

A3 Data set combination

The combination is based on monthly zonal mean time series from the individual data sets. In the overlap period a time-independent shift is determined that minimises the offset between the time series in a root mean square sense. This shift is derived for every altitude level and latitude bin considered and subsequently applied to the MIPAS time series. Applications of the combined HALOE-MIPAS time series can be found in Eichinger et al. (2014) or Schieferdecker et al. (2015).

A4 Analysis approach

The basic data for the analysis are monthly zonal mean data covering the time period from July 1998 to December 2005. The HALOE-MIPAS data set is interpolated in time to fill a few gaps. The data are averaged over a latitude range of 20° using a 10° latitude grid. The rather wide average in latitude aims to handle some of the sparseness of the HALOE observations. For the simulations this would not be necessary but for reasons of compatibility and comparability the same handling is applied. In the vertical the data sets extend from 100 to about 7 hPa and are interpolated on a regular grid using 16 levels per pressure decade.

The analysis is performed separately for every pressure level and latitude bin using the steps listed below. Figure A1 shows an example.

In a first step we calculate a running average over one year. In Fig. A1 the averaged time series is given by the black line. Based on that time series we calculate in the next step the gradient in water vapour along every data point.

ACPD
15, 24909–24953, 2015

Subsequently we look for periods with sequences of at least six data points that have a negative gradient allowing one data point in-between to have a positive or zero gradient. Typically we find several of such periods, as seen in the example in Fig. A1. We only consider those periods that have started within a certain time interval. For 100 hPa this interval ranges from January 2000 to January 2004, as indicated by the red lines in Fig. A1. This is based on a priori knowledge. For higher altitudes we adjust the start of the interval to the start date of the millennium drop at 100 hPa. At this altitude the drop is typically easiest to observe and we expect that higher up no earlier start dates occur.

To decide which of the periods represents the millennium drop we rely on two parameters, one, the absolute change in water vapour and, two, its overall gradient. These parameters are calculated for every period. Subsequently the periods are ranked according to these parameters with the largest absolute value gaining the highest rank. The ranks for a period are summed up and the period with the lowest sum is considered as the period that most likely represents the millennium drop. In the example shown in Fig. A1 the first period is chosen to represent the millennium drop as it exhibits both the largest decrease and the strongest negative gradient among the possible periods.

Author contributions. S. Brinkop prepared the manuscript and analyzed the model data. M. Dameris was involved in the discussion of the data analysis results and supported the writing of the manuscript. H. Garny calculated the residual circulation based on the model simulations. P. Jöckel performed the simulations with EMAC. G. Stiller provided the MIPAS data and participated in the discussion. S. Lossow performed the novel analysis of the water vapor drop characteristics with the HALOE/MIPAS and the model simulation data.

Acknowledgements. This work has been funded by the Deutsche Forschungsgemeinschaft (DFG) within the research unit Stratospheric Change and its Role for Climate Prediction (SHARP-FOR 1095). The presented investigations were carried out within the water vapour project SHARP-WV. The model simulations were performed within the DKRZ project ESCiMo (Earth System Chemistry integrated Modelling). We would like to thank the Deutsches Klimarechenzentrum (DKRZ) for providing computing time and support and Christoph Kiemle for valuable comments on the manuscript.

ACPD
15, 24909–24953, 2015

The article processing charges for this open-access publication were covered by a Research Centre of the Helmholtz Association.

References

Calvo, N., Garcia, R. R., Randel, W. J., and Marsh, D. R.: Dynamical mechanism for the increase in tropical upwelling in the lowermost tropical stratosphere during warm ENSO events, J. Atmos. Sci., 67, 2331–2340, 2010.

Deckert, R. and Dameris, M.: Higher tropical SSTs strengthen the tropical upwelling via deep convection, Geophys. Res. Lett., 35, L10813, doi:10.1029/2008GL033719, 2008.

Eichinger, R., Jöckel, P., and Lossow, S.: Simulation of the isotopic composition of stratospheric water vapour – Part 2: Investigation of HDO/H_2O variations, Atmos. Chem. Phys., 15, 7003–7015, doi:10.5194/acp-15-7003-2015, 2015.

Eyring, V. and Lamarque, J.-F.: Global chemistry-climate modeling and evaluation, EOS Trans. AGU, 93, 539, doi:10.1029/2012EO510012, 2012.

Fischer, H., Birk, M., Blom, C., Carli, B., Carlotti, M., von Clarmann, T., Delbouille, L., Dudhia, A., Ehhalt, D., Endemann, M., Flaud, J. M., Gessner, R., Kleinert, A., Koopman, R., Langen, J., López-Puertas, M., Mosner, P., Nett, H., Oelhaf, H., Perron, G., Remedios, J., Ridolfi, M., Stiller, G., and Zander, R.: MIPAS: an instrument for atmospheric and climate research, Atmos. Chem. Phys., 8, 2151–2188, doi:10.5194/acp-8-2151-2008, 2008.

Fueglistaler, S., Bonazzola, M., Haynes, P., and Peter, T.: Stratospheric water vapor predicted from the Lagrangian temperature history of air entering the stratosphere in the tropics, J. Geophys. Res., 110, D08107, doi:10.1029/2004JD005516, 2005.

Fueglistaler, S., Liu, Y. S., Flannaghan, T. J., Haynes, P. H., Dee, D. P., Read, W. J., Remsberg, E. E., Thomason, L. W., Hurst, D. F., Lanzante, J. R., and Bernath, P. F.: The relation between atmospheric humidity and temperature trends for stratospheric water, J. Geophys. Res., 118, 1052–1074, doi:10.1002/jgrd.50157, 2013.

Gettelman, A., Birner, T., Eyring, V., Akiyoshi, H., Bekki, S., Brühl, C., Dameris, M., Kinnison, D. E., Lefevre, F., Lott, F., Mancini, E., Pitari, G., Plummer, D. A., Rozanov, E., Shibata, K., Stenke, A., Struthers, H., and Tian, W.: The Tropical Tropopause Layer 1960–2100, Atmos. Chem. Phys., 9, 1621–1637, doi:10.5194/acp-9-1621-2009, 2009.

ACPD
15, 24909–24953, 2015

Hartmann, D. L., Klein Tank, A. M. G., Rusticucci, M., Alexander, L. V., Brönnimann, S., Charabi, Y., Dentener, F. J., Dlugokencky, E. J., Easterling, D. R., Kaplan, A., Soden, B. J., Thorne, P. W., Wild, M., and Zhai, P. M.: Observations: Atmosphere and Surface, in: Climate Change 2013: The Physical Science Basis. Contribution of Working Group I to the Fifth Assessment Report of the Intergovernmental Panel on Climate Change, edited by: Stocker, T. F., Qin, D., Plattner, G.-K., Tignor, M., Allen, S. K., Boschung, J., Nauels, A., Xia, Y., Bex, V., and Midgley, P. M., Cambridge University Press, Cambridge, UK, and New York, NY, USA, 2013.

Hegglin, M. I., Tegtmeier, S., Anderson, J., Froidevaux, L., Fuller, R., Funke, B., Jones, A., Lingenfelser, G., Lumpe, J., Pendlebury, D., Remsberg, E., Rozanov, A., Toohey, M., Urban, J., von Clarmann, T., Walker, K. A., Wang, R., and Weigel, K.: SPARC Data Initiative: Comparison of water vapor climatologies from international satellite limb sounders, J. Geophys. Res.-Atmos., 118, 11824–11846, doi:10.1002/jgrd.50752, 2013.

Hegglin, M. I., Plummer, D. A., Shepherd, T. G., Scinocca, J. F., Anderson, J., Froidevaux, L., Funke, B., Hurst, D., Rozanov, A., Urban, J., von Clarmann, T., Walker, K. A., Wang, H. J., Tegtmeier, S., and Weigel, K.: Vertical structure of stratospheric water vapour trends derived from merged satellite data, Nat. Geosci., 7, 768–776, 2014.

Holton, J. R.: An Introduction to Dynamic Meteorology, International Geophysics Series, 4th edn., Academic Press, San Diego, New York, USA, 2004.

Hurst, D. F., Oltmans, S. J., Vömel, H., Rosenlof, K. H., Davis, S. M., Ray, E. A., Hall, E. G., and Jordan, A. F.: Stratospheric water vapor trends over Boulder, Colorado: analysis of the 30 year boulder record, J. Geophys. Res., 116, D02306, doi:10.1029/2010JD015065, 2011.

Jöckel, P., Kerkweg, A., Pozzer, A., Sander, R., Tost, H., Riede, H., Baumgaertner, A., Gromov, S., and Kern, B.: Development cycle 2 of the Modular Earth Submodel System (MESSy2), Geosci. Model Dev., 3, 717–752, doi:10.5194/gmd-3-717-2010, 2010.

Jöckel, P., Tost, H., Pozzer, A., Kunze, M., Kirner, O., Brinkop, S., Cai, D. S., Frank, F., Garny, H., Gottschaldt, K.-D., Graf, P., Grewe, V., Kern, B., Matthes, S., Mertens, M., Meul, S., Nützel, M., Oberländer-Hayn, S., Ruhnke, R., Runde, T., and Sander, R.: Earth System Chemistry Integrated Modelling (ESCiMo) with the Modular Earth Submodel System (MESSy, version 2.51), Geosci. Model Dev., submitted, 2015.

Jones, C. D., Hughes, J. K., Bellouin, N., Hardiman, S. C., Jones, G. S., Knight, J., Liddicoat, S., O'Connor, F. M., Andres, R. J., Bell, C., Boo, K.-O., Bozzo, A., Butchart, N., Cadule, P., Corbin, K. D., Doutriaux-Boucher, M., Friedlingstein, P., Gornall, J., Gray, L., Halloran, P. R., Hurtt, G., Ingram, W. J., Lamarque, J.-F., Law, R. M., Meinshausen, M.,

ACPD
15, 24909–24953, 2015

Osprey, S., Palin, E. J., Parsons Chini, L., Raddatz, T., Sanderson, M. G., Sellar, A. A., Schurer, A., Valdes, P., Wood, N., Woodward, S., Yoshioka, M., and Zerroukat, M.: The HadGEM2-ES implementation of CMIP5 centennial simulations, Geosci. Model Dev., 4, 543–570, doi:10.5194/gmd-4-543-2011, 2011.

Kley, D., Russell, J. M., and Philips, C.: Stratospheric Processes and their Role in Climate (SPARC) – Assessment of Upper Tropospheric and Stratospheric Water Vapour, SPARC Report 2, WMO/ICSU/IOC World Climate Research Programme, Geneva, Switzerland, 2000.

Maycock, A. C., Joshi, M. M., Shine, K. P., Davis, S. M., and Rosenlof, K. H.: The potential impact of changes in lower stratospheric water vapour on stratospheric temperatures over the past 30 years, Q. J. Roy. Meteor. Soc., 140, 2176–2185, doi:10.1002/qj.2287, 2014.

Mote, P. W., Rosenlof, K. H., Holton, J. R., Harwood, R. S., and Waters, J. W.: An atmospheric tape recorder: the imprint of tropical tropopause temperatures on stratospheric water vapor, J. Geophys. Res., 101, 3989–4006, 1996.

Randel, W. J. and Jensen, E. J.: Physical processes in the tropical tropopause layer and their roles in a changing climate, Nat. Geosci., 6, 169–176, doi:10.1038/ngeo1733, 2013.

Randel, W. J., Wu, F., Oltmans, S. J., Rosenlof, K., and Nedoluha, G.: Interannual changes of stratospheric water vapor and correlations with tropical tropopause temperatures, J. Atmos. Sci., 61, 2133–2148, 2004.

Randel, W. J., Wu, F., Vömel, H., Nedoluha, G. E., and Forster, P.: Decreases in stratospheric water vapor after 2001: links to changes in the tropical tropopause and the Brewer–Dobson circulation, J. Geophys. Res., 111, D12312, doi:10.1029/2005JD006744, 2006.

Randel, W. J., Garcia, R. R., Calvo, N., and Marsh, D.: ENSO influence on zonal mean temperature and ozone in the tropical lower stratosphere, Geophys. Res.Lett, 36, L15822, doi:10.1029/2009GL039343, 2009.

Roeckner, E., Brokopf, R., Esch, M., Giorgetta, M., Hagemann, S., Kornblueh, L., Manzini, E., Schlese, U., and Schulzweida, U.: Sensitivity of simulated climate to horizontal and vertical resolution in the ECHAM5 atmosphere model, J. Climate, 19, 3771–3791, doi:10.1175/JCLI3824.1, 2006.

Rosenlof, K. H. and Reid, G. C.: Trends in the temperature and water vapor content of the tropical lower stratosphere: sea surface connection, J. Geophys. Res., 113, D06107, doi:10.1029/2007JD009109, 2008.

ACPD
15, 24909–24953, 2015

Russell, J. M., Gordley, L. L., Park, J. H., Drayson, S. R., Hesketh, W. D., Cicerone, R. J., Tuck, A. F., Frederick, J. E., Harries, J. E., and Crutzen, P. J.: The halogen occultation experiment, J. Geophys. Res., 98, 10777–10797, 1993.

Scherer, M., Vömel, H., Fueglistaler, S., Oltmans, S. J., and Staehelin, J.: Trends and variability of midlatitude stratospheric water vapour deduced from the re-evaluated Boulder balloon series and HALOE, Atmos. Chem. Phys., 8, 1391–1402, doi:10.5194/acp-8-1391-2008, 2008.

Schieferdecker, T.: Variabilität von Wasserdampf in der unteren und mittleren Stratosphäre auf der Basis von HALOE/UARS und MIPAS/Envisat Beobachtungen, PhD thesis, Karlsruhe Institute oft Technology, available at: http://digbib.ubka.uni-karlsruhe.de/volltexte/1000046296, last access: 22 June 2015.

Schieferdecker, T., Lossow, S., Stiller, G. P., and von Clarmann, T.: Is there a solar signal in lower stratospheric water vapour?, Atmos. Chem. Phys., 15, 9851–9863, doi:10.5194/acp-15-9851-2015, 2015.

Schoeberl, M. R., Dessler, A. E., and Wang, T.: Simulation of stratospheric water vapor and trends using three reanalyses, Atmos. Chem. Phys., 12, 6475–6487, doi:10.5194/acp-12-6475-2012, 2012.

Shepherd, T. G. and McLandress, C.: A robust mechanism for strengthening of the Brewer–Dobson circulation in response to climate change: critical-layer control of subtropical wave breaking, J. Atmos. Sci., 68, 784–797, doi:10.1175/2010JAS3608.1, 2011.

Solomon, S., Rosenlof, K. H., Portmann, R. W., Daniel, J. S., Davis, S. M., Sanford, T. S., and Plattner, G.-K.: Contributions of stratospheric water vapor to decadal changes in the rate of global warming, Science, 327, 1219–1223, doi:10.1126/science.1182488, 2010.

SPARC CCMVal (Stratospheric Processes And their Role in Climate): SPARC Report on the Evaluation of Chemistry-Climate Models, edited by: Eyring, V., Shepherd, T. G., and Waugh, D. W., SPARC Report No. 5, WCRP-132, WMO/TD-No. 1526, 478 pp., available at: http://www.atmosp.physics.utoronto.ca/SPARC/ccmval_final/index.php (last access: 22 June 2015), 2010.

Stenke, A. and Grewe, V.: Simulation of stratospheric water vapor trends: impact on stratospheric ozone chemistry, Atmos. Chem. Phys., 5, 1257–1272, doi:10.5194/acp-5-1257-2005, 2005.

Urban, J., Lossow, S., Stiller, G., and Read, W.: Another drop in water vapor, EOS, 95, 245–246, 2014.

ACPD
15, 24909–24953, 2015

Wang, L., Zou, C.-Z., and Qian, H.: Constructions of stratospheric temperature data records from Stratospheric Sounding Units, J. Climate, 25, 2931–2946, doi:10.1175/JCLI-D-11-00350.1, 2012.

WMO (World Meteorological Organization), Scientific Assessment of Ozone Depletion: 2014, Global Ozone Research and Monitoring Project – Report No. 55, 416 pp., Geneva, Switzerland, 2014.

ACPD

15, 24909–24953, 2015

Table 1. Correlation of anomalies (de-trended, de-seasonalised) for RC1SD, RC1 and RC2 at 90 and 70 hPa, respectively.

Correlation of anomalies	1980–2012 RC1SD 70 hPa	1960–2011 RC1 70 hPa	1960–2030 RC2 70 hPa	1980–2012 RC1SD 90 hPa	1960–2011 RC1 90 hPa	1960–2030 RC2 90 hPa
Temperature-ozone	0.69	0.92	0.88	0.60	0.70	0.41
Temperature-upwelling	−0.70	−0.55	−0.44	−0.64	−0.61	−0.39
Temperature-QBO	0.42	0.52	0.47	0.25	−0.25	−0.12
Ozone-upwelling	−0.56	−0.62	−0.54	−0.54	−0.65	−0.45
Ozone-QBO	0.51	0.57	0.50	0.23	−0.38	−0.14
Temperature-moisture	0.37	0.84	0.80	0.86	0.94	0.90

ACPD
15, 24909–24953, 2015

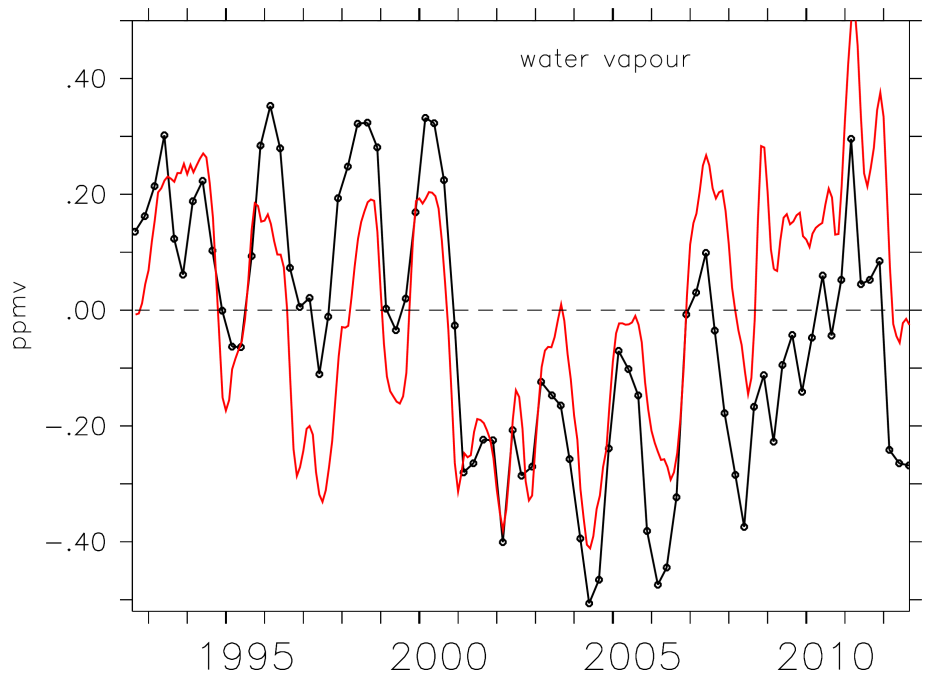

Figure 1. Interannual changes of the near-global mean (60° S–60° N) stratospheric water vapour mixing ratios (in ppmv) at 83 hPa. The black line is the data derived from satellite observations (combined HALOE and Aura/MLS satellite measurements, de-seasonalised, 3 month running mean), which was published by Randel and Jensen (2013) in their Fig. 5a (upper graph). The red line is the RC1SD simulation (de-seasonalised, 3 month running mean).

ACPD
15, 24909–24953, 2015

The millennium water vapour drop in chemistry-climate model simulations

S. Brinkop et al.

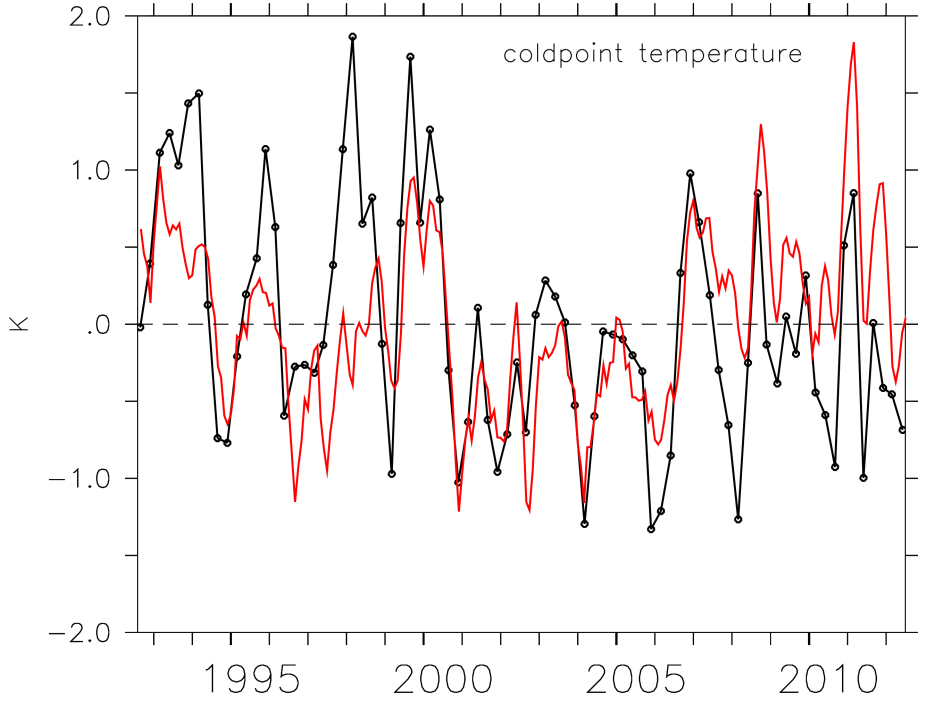

Figure 2. Cold point temperatures in the tropics (20° S–20° N) derived from radiosonde data (black line). The data was already published by Randel and Jensen (2013) in their Fig. 5a (lower graph). The red line is the RC1SD simulation (de-seasonalised, 3 month running mean).

ACPD
15, 24909–24953, 2015

The millennium water vapour drop in chemistry-climate model simulations

S. Brinkop et al.

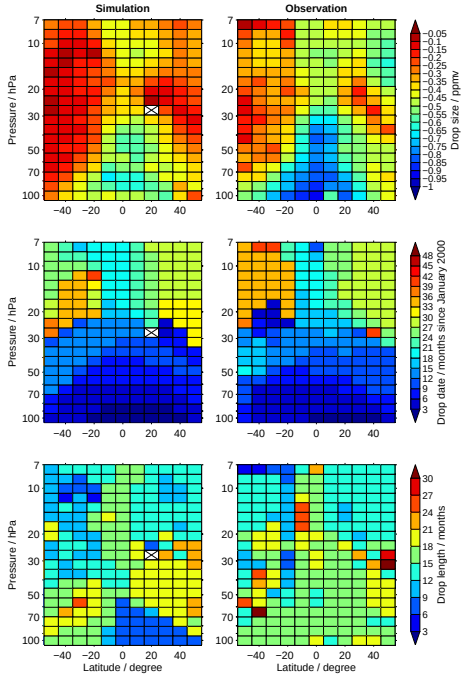

Figure 3. Characteristics of the millennium water vapour drop with respect to height (hPa). RIGHT: Satellite observations. LEFT: RC1SD simulation. TOP: Drop strength (unit: ppmv), MIDDLE: drop date (months since January 2000). BOTTOM: drop length (unit: months). White boxes with crosses indicate that the analysis failed to find a water vapour decrease that fulfilled the criteria listed in the Appendix.

ACPD
15, 24909–24953, 2015

The millennium water vapour drop in chemistry-climate model simulations

S. Brinkop et al.

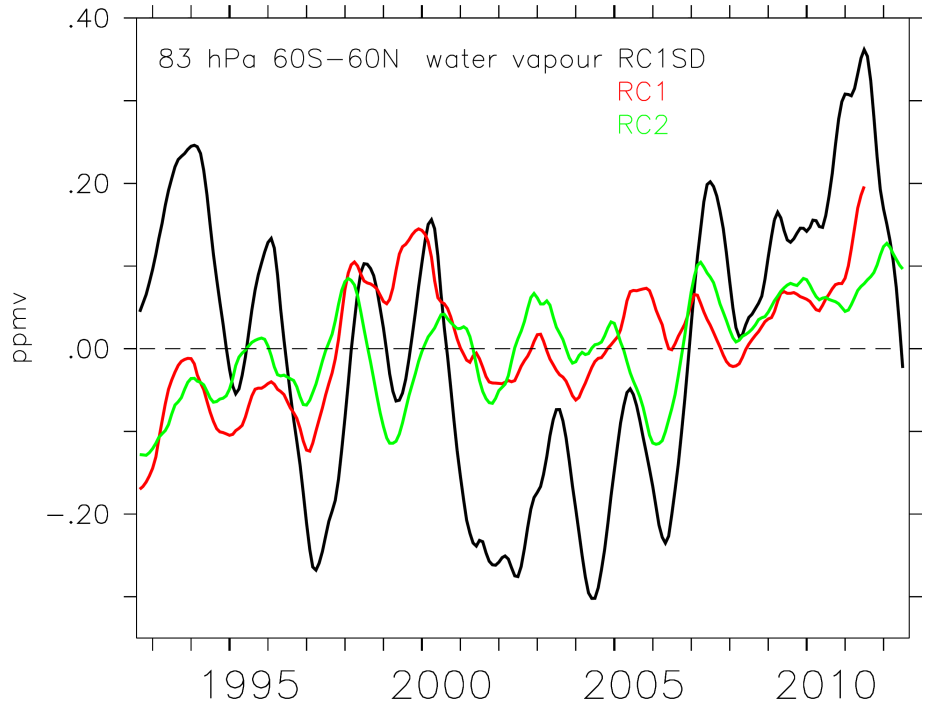

Figure 4. Near-global mean (60° S–60° N) water vapour anomalies (de-seasonalised, note, these anomalies are a 12 month running mean and therefore slightly different compared to RC1SD in Fig. 1) derived from RC1SD, RC1 and RC2 simulations.

ACPD
15, 24909–24953, 2015

The millennium water vapour drop in chemistry-climate model simulations

S. Brinkop et al.

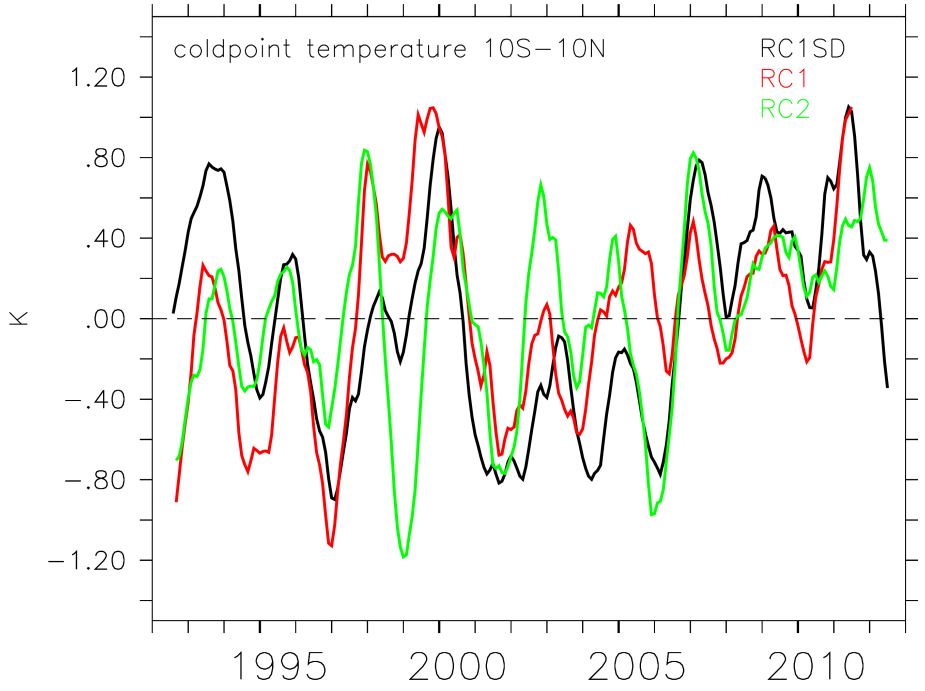

Figure 5. Cold point temperature anomalies (de-seasonalised, 12 month running mean) derived from RC1SD, RC1 and RC2 simulations.

ACPD
15, 24909–24953, 2015

The millennium water vapour drop in chemistry-climate model simulations

S. Brinkop et al.

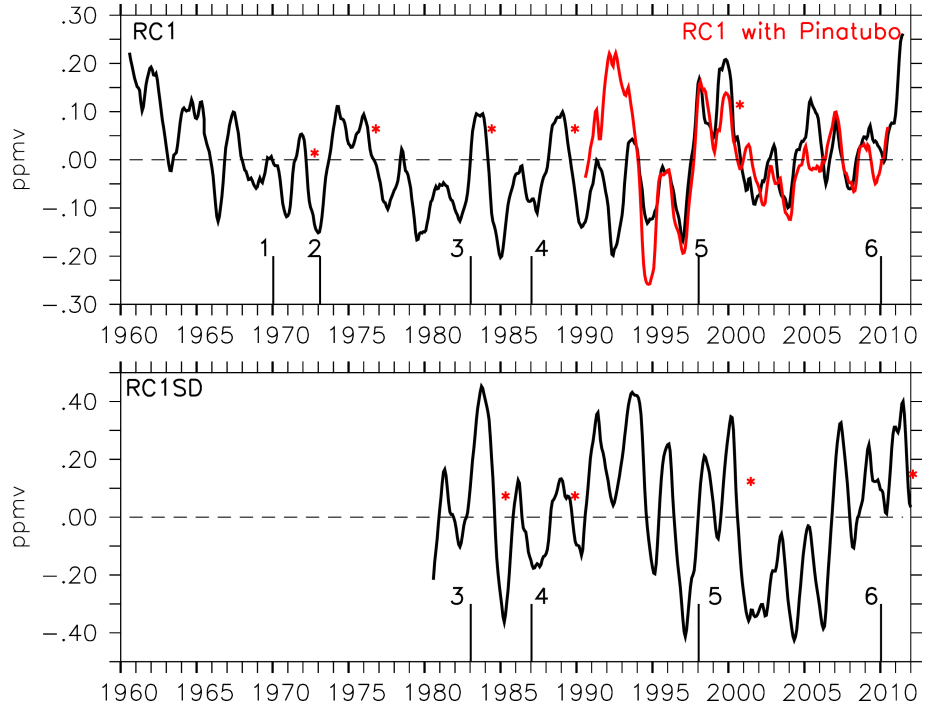

Figure 6. Moisture anomalies in ppmv (detrended, de-seasonalised, 12-months running mean) derived from RC1SD and RC1 simulations at 80 hPa. Black vertical lines mark El Niño events and red asterisks mark the respective subsequent water vapour drop.

ACPD
15, 24909–24953, 2015

The millennium water vapour drop in chemistry-climate model simulations

S. Brinkop et al.

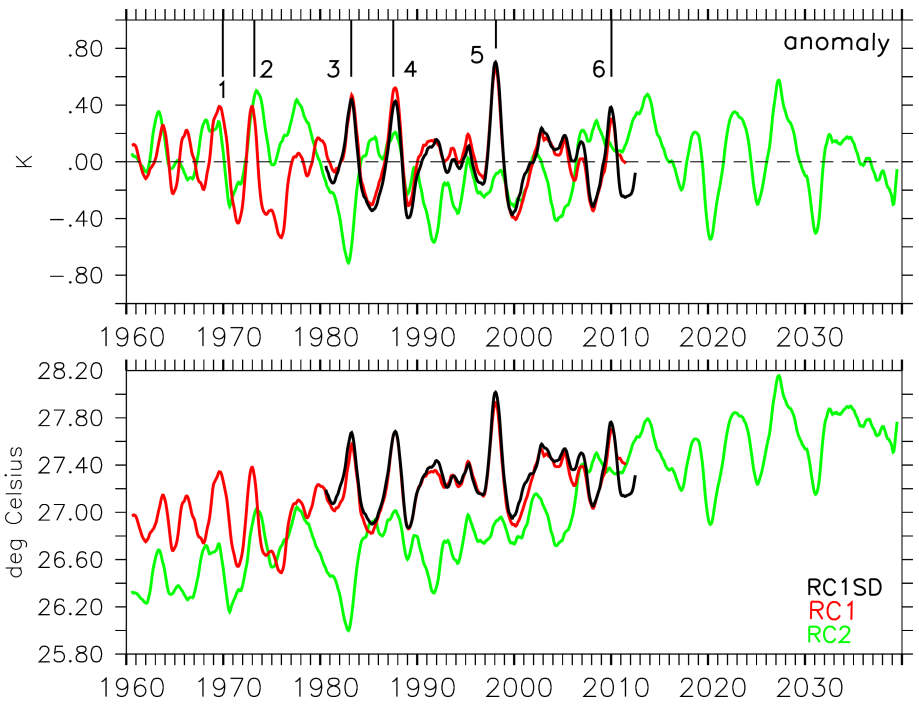

Figure 7. (a) Surface temperature anomaly in the tropical region (10° S–10° N) (de-trended, de-seasonalised, 12-point running mean) for RC1SD (black), RC1 (red) and RC2 (green). Strong El Niño/La-Niña events are labeled. **(b)** Surface temperature (degree Celsius) for RC1SD, RC1 and RC2 (12-point running mean).

ACPD
15, 24909–24953, 2015

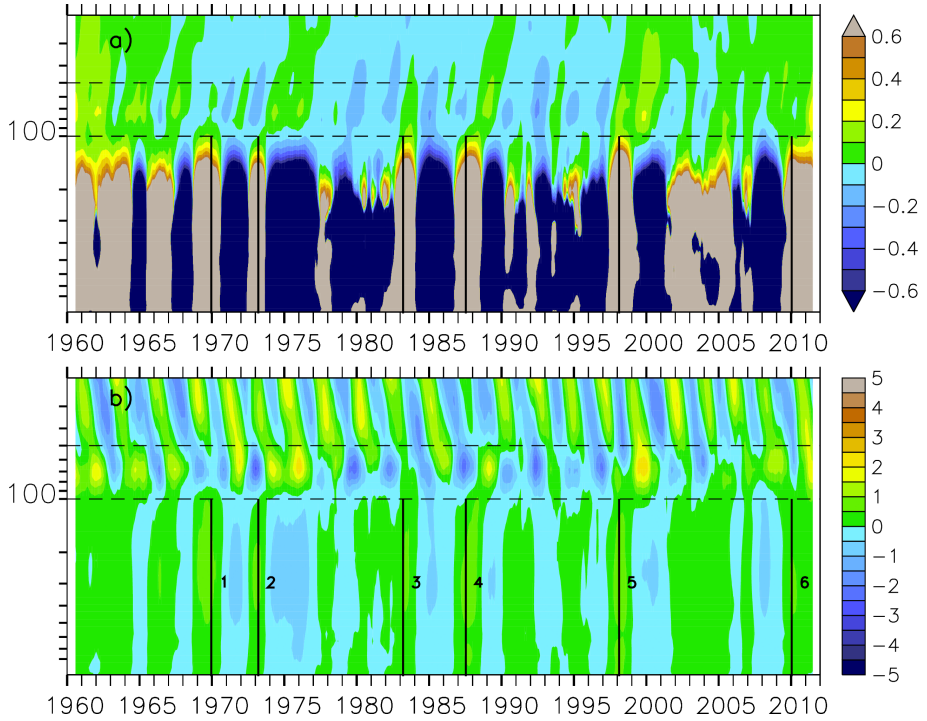

Figure 8. (a) Temporal evolution of moisture anomalies (ppmv). **(b)** Temporal evolution of temperature anomalies (K) in the tropical UTLS region (12 month running mean), derived from the RC1 simulation. Strong El Niño events are labelled. The altitude range covers the pressure levels from 900 to 30 hPa. The dashed lines mark the region between 100 and 50 hPa.

ACPD
15, 24909–24953, 2015

The millennium water vapour drop in chemistry-climate model simulations

S. Brinkop et al.

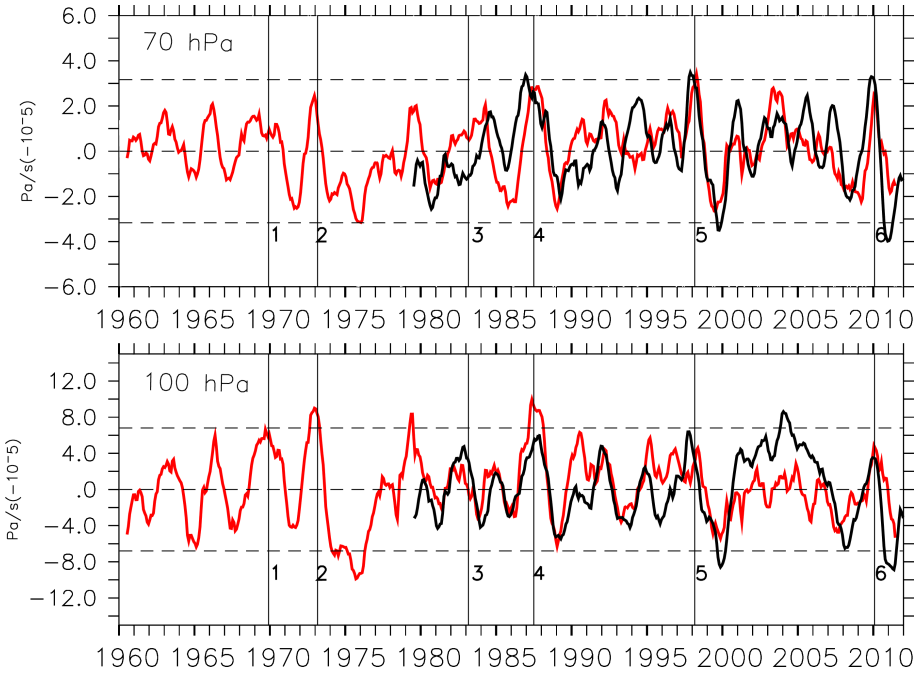

Figure 9. Temporal evolution of tropical upwelling anomalies in the tropics (20° S–20° N) (deseaonalised and detrended) at 70 and 100 hPa (running mean). Red lines indicate data derived from RC1, black lines from RC1SD. Black dashed lines mark one standard deviation from the unsmoothed RC1SD monthly mean upwelling anomaly values. Black solid vertical lines mark El Niño events.

ACPD
15, 24909–24953, 2015

The millennium water vapour drop in chemistry-climate model simulations

S. Brinkop et al.

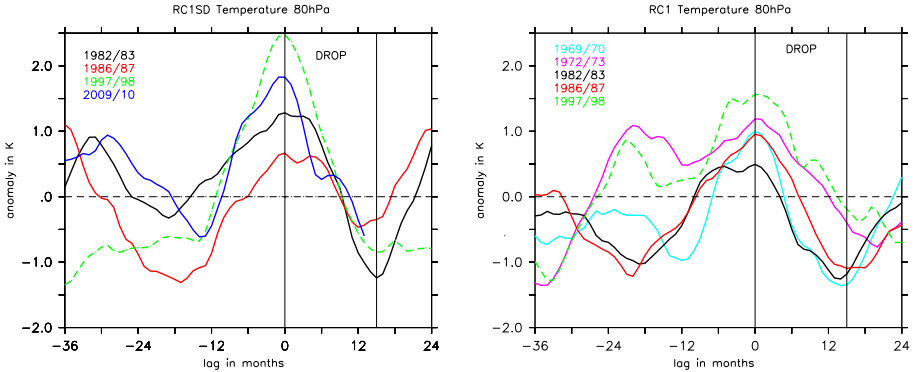

Figure 10. Episode analysis of the zonal mean temperature anomaly at 80 hPa, tropical mean (10° S–10° N), de-seasonalized, de-trended, 12-point running mean, related to 4 different El Niño events in the RC1SD (left) and the RC1 (right) simulation. All episodes are referenced to the beginning of the respective temperature drop.

ACPD
15, 24909–24953, 2015

The millennium water vapour drop in chemistry-climate model simulations

S. Brinkop et al.

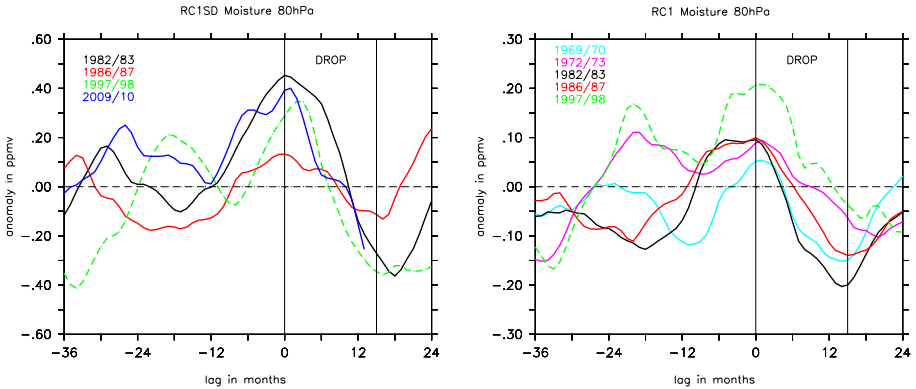

Figure 11. Same as Fig. 10, but for the water vapour anomaly. Note that the vertical axis is smaller in the right figure.

ACPD
15, 24909–24953, 2015

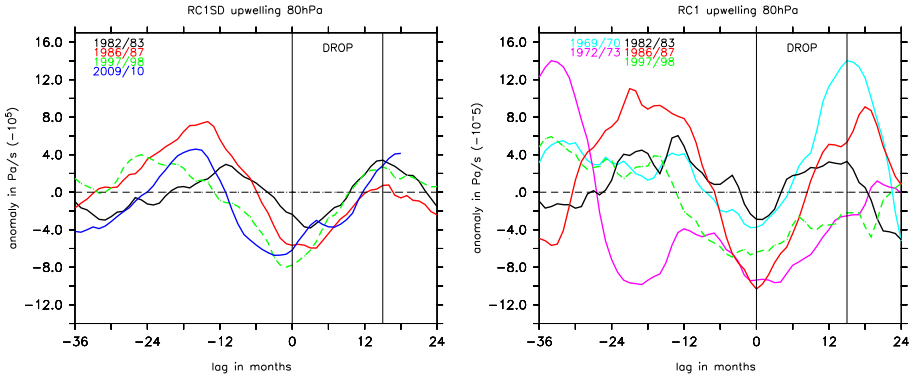

Figure 12. Same as Fig. 10, but for tropical upwelling anomaly.

ACPD
15, 24909–24953, 2015

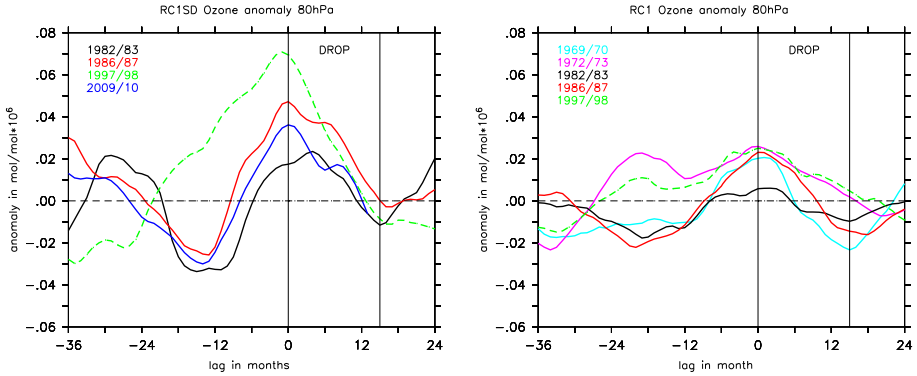

Figure 13. Same as Fig. 10, but for the ozone anomaly.

ACPD
15, 24909–24953, 2015

The millennium water vapour drop in chemistry-climate model simulations

S. Brinkop et al.

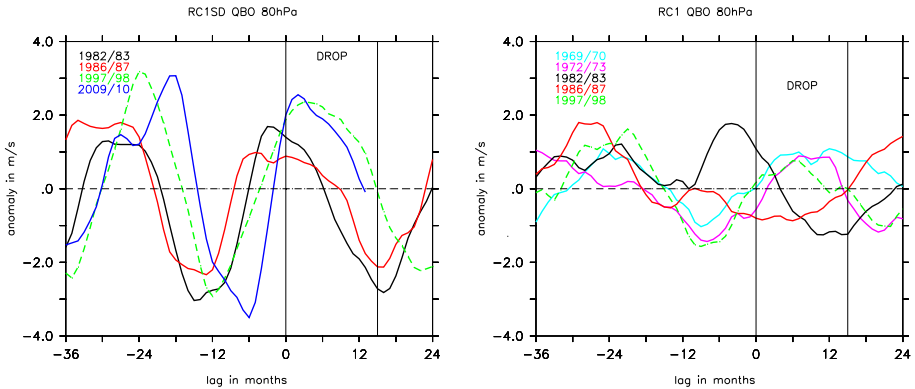

Figure 14. Same as Fig. 10, but for the QBO anomaly. The QBO is represented through the zonal wind anomaly.

ACPD
15, 24909–24953, 2015

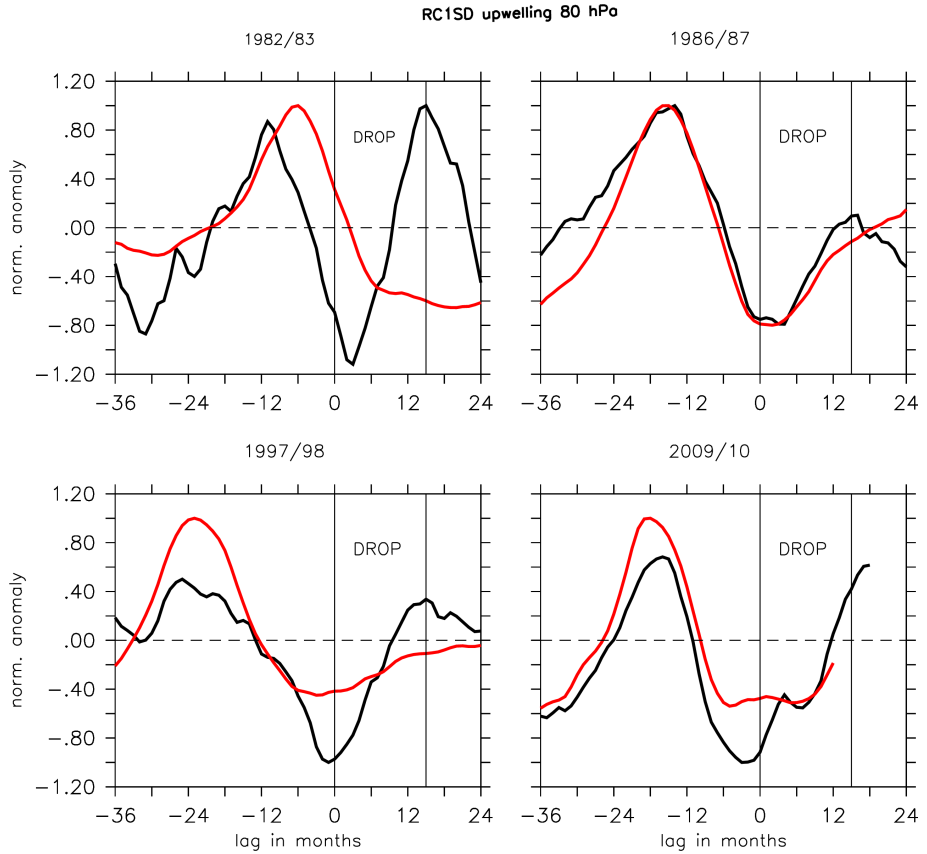

Figure 15. Episode analysis for the normalised (with respect to the maximum absolute value) upwelling anomaly (black) for (10° N–10° S) in relation to the max-normalised SST anomaly for the El Niño index 3.4 region. All episodes are referenced to the beginning of the temperature drop. The drop onsets are accompanied by a negative upwelling anomaly.

ACPD
15, 24909–24953, 2015

The millennium water vapour drop in chemistry-climate model simulations

S. Brinkop et al.

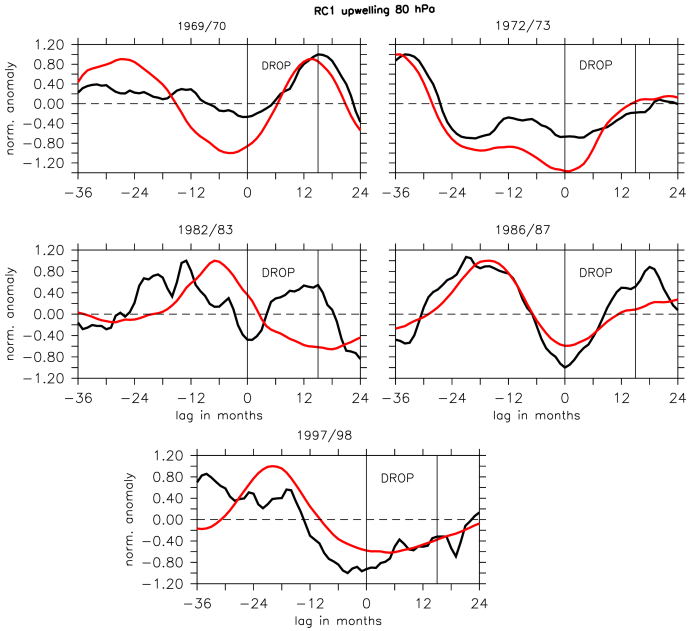

Figure 16. Episode analysis for the normalised (with respect to the maximum absolute value) upwelling anomaly (black) for (10° S–10° N) in relation to the max-normalised SST anomaly for the El Niño index 3.4 region. All episodes are referenced to the beginning of the temperature drop. The drop onsets are accompanied by a negative upwelling anomaly. The El Niño event in 1972/73 (red line) starts already before the month −36. This event has the largest delay of the drop after the surface temperature maximum for all analysed events.

ACPD
15, 24909–24953, 2015

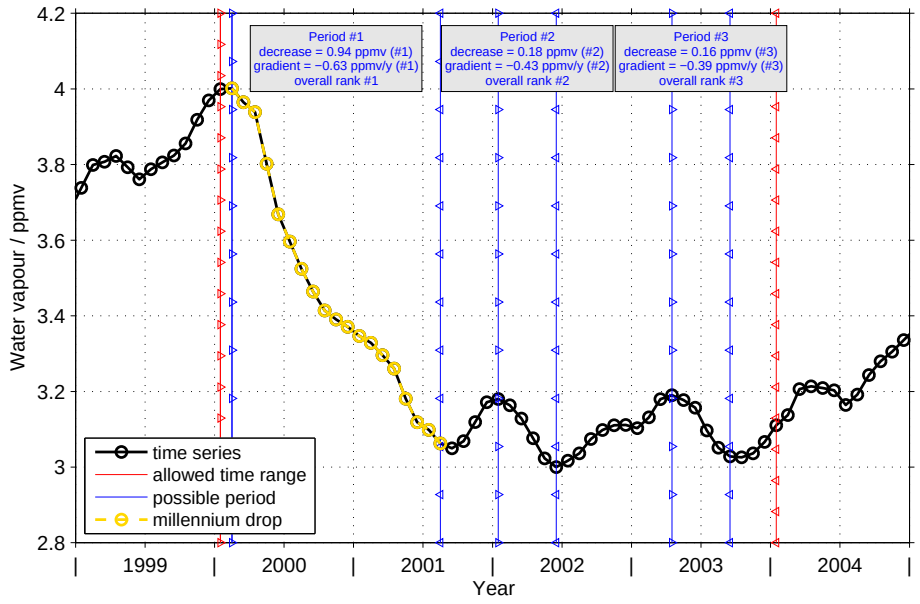

Figure A1. An example of the millennium drop characteristics analysis considering the HALOE/MIPAS time series at 100 hPa at the Equator. The time series is given in black and represents a running mean over one year. The red lines indicate the general time interval where a water vapour drop will be considered. Within this period three periods can be found where water vapour is decreasing. The first period from February 2000 to August 2001 (overplotted in yellow) exhibits both the largest decrease and absolute gradient and is therefore selected as the representative period for the millennium drop.

ACPD
15, 24909–24953, 2015